NJC

Accepted Manuscript

This is an *Accepted Manuscript*, which has been through the Royal Society of Chemistry peer review process and has been accepted for publication.

Accepted Manuscripts are published online shortly after acceptance, before technical editing, formatting and proof reading. Using this free service, authors can make their results available to the community, in citable form, before we publish the edited article. We will replace this *Accepted Manuscript* with the edited and formatted *Advance Article* as soon as it is available.

You can find more information about *Accepted Manuscripts* in the Information for Authors.

Please note that technical editing may introduce minor changes to the text and/or graphics, which may alter content. The journal's standard Terms & Conditions and the Ethical guidelines still apply. In no event shall the Royal Society of Chemistry be held responsible for any errors or omissions in this *Accepted Manuscript* or any consequences arising from the use of any information it contains.

ROYAL SOCIETY OF CHEMISTRY

www.rsc.org/njc

Journal Name

RSCPublishing

ARTICLE

Nonstoichiometric $Cu_{2-x}Se$ nanocrystals in situ produced on the surface of carbon nanotubes for ablation of tumor cells

Cite this: DOI: 10.1039/x0xx00000x

Received 00th January 2012,
Accepted 00th January 2012

DOI: 10.1039/x0xx00000x

www.rsc.org/

Qiang Wang,[a] Wen Long Li,[b] Hong Yan Zou,[b] Hui Liu*[a] and Cheng Zhi Huang*[ab]

Carbon nanotubes (CNTs) are well known as photo-thermal agents for ablation of tumor cells, but limited in the application in photo-thermal therapy (PTT) owing to their low molar extinctions. By coupling the photo-thermal effects of CNTs and the intense localized surface plasmon resonance (LSPR) in the near-infrared (NIR) region of $Cu_{2-x}Se$ nanoparticles (NPs), herein we developed a high efficient PTT nanohybrids agent by *in situ* growth of $Cu_{2-x}Se$ NPs on the acid-functionalized CNTs at room temperature, and the as-prepared $Cu_{2-x}Se$/CNTs nanohybrids have been found to have intense LSPR in NIR and an well photo-thermal conversion property. Moreover, possessing good biocompatibility and dispersibility, the nanohybrids could easily be internalized by cancer cells, and show smart photo-thermal performance, which were then successfully applied for photo-thermal therapy *in vitro*, indicating that the $Cu_{2-x}Se$/CNTs nanohybrids could be a potential photo-thermal therapy agent for ablation of tumor cells.

Introduction

Photo-thermal therapy (PTT) as a promising and effective way for target cell death has been widely studied in the past decade.[1, 2] On one hand, it is a hyperthermia therapeutic method that converts near-infrared (NIR) absorption to high temperature and further change the cellular microenvironment to promote apoptosis.[3] The NIR light (700~1400 nm) has a strong ability to penetrate biological tissue due to the low adsorption of biological tissue.[4] On the other hand, nanomaterials could be accumulated in tumour tissues by enhanced permeability and retention (EPR) effect.[5] Therefore, various types of nanomaterials with intense NIR absorption ability have been applied for PTT.

Photo-thermal agents up to now have been reported for cancer treatment mainly include four types of materials. The first type is the carbon-based materials, such as graphene oxide (GO) and carbon nanotubes (CNTs), exhibiting unique physical and chemical properties which have been extensively utilized as plasmon probes for the delivery of large biomolecules and PTT owing to their biocom-patibility and optical properties,[6-9] However, these materials show a low extinction coefficient (CNTs, 4.4×10^3 $M^{-1}\cdot cm^{-1}$) for photo-thermal treatment compared with Au NPs, which limit their wide application in biomedicine.[10, 11] The second type is the NIR-absorbing organic compounds, including polyaniline, polypyrrole and indocyanine green (ICG) dye and so on.[12, 13] Although the organic polymer have been used for drug delivery and cancer therapy, it still suffer from serious low PTT efficacy and photo-bleaching. The third type of photo-thermal agent is metal materials involved in Au nanostructures and Pd nanosheets. Based on their surface plasmon resonance properties and the molar extinction coefficient of 10^8~10^{11} $M^{-1}\cdot cm^{-1}$,[14, 15] these metal materials show excellent photo-thermal conversion efficiency, for example Au nanoshells (13%) and Au nanorods (21%).[16] However, the noble metal based photo-thermal agent is so expensive and have some cellular toxicity. The last type is copper sulfide and copper selenide nanocrystals, which as low-cost, earth-abundant, ecofriendly semiconductors show a well-defined LSPR in the NIR region owing to the presence of copper deficiencies in NPs[17-20] and have been applied in photo-acoustic imaging and photo-thermal therapy.[16, 21, 22] In addition, copper chalcogenide NCs, owing to the higher photo-thermal conversion efficiency ($Cu_{2-x}Se$, 22%; Cu_9S_5, 25.7%) and low cytotoxicity,[16, 23] might become an ideal PTT agent. Since the carbon-based nanocomposites have been explored for exhibiting better performance than individual one and could exploit different material properties together in nanomedicine applications,[8, 9, 24] making some efforts therefore to study the capability of copper chalcogenide /CNTs hybrids is far-reaching for good applications in biomedical fields.

Based on the characteristics of above PTT agent, we develop a water-phase approach for facile synthesis of.

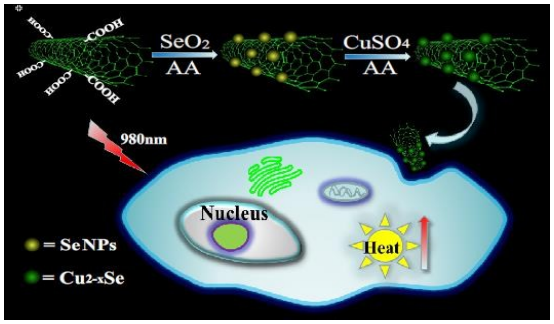

Scheme 1. Illustration of the preparation and application of $Cu_{2-x}Se$/CNTs nanohybrids as for cancer treatment.

copper selenide/carbon nanotubes ($Cu_{2-x}Se$/CNTs) nano-hybrids at room temperature, which show very smart photo-thermal conversion performance for PTT since it has combined the photo-thermal features of CNTs and the intense LSPR of $Cu_{2-x}Se$ nanocrystals in NIR. The $Cu_{2-x}Se$ NPs are *in situ* reduced on the surface of CNTs by ascorbic acid and uniformly loaded on the CNTs without aggregation. The acid functionalized CNTs as a stabilizer have sufficient carboxyl groups on the defect sites and the tube ends to binding $Cu_{2-x}Se$ NPs. The surface modification of CNTs make the $Cu_{2-x}Se$/CNTs nanohybrids possess excellent biocompatibility and dispersibility for intracellular transport. It is in line with expectations that the nanohybrids have a well-defined NIR absorption and the combinations of $Cu_{2-x}Se$ NPs and CNTs can improve the photo-thermal efficiency as therapeutic agents. Therefore, the as-prepared $Cu_{2-x}Se$/CNTs nanohybrids can become a potential agent for photo-thermal therapy

Experimental Section

Chemicals and Materials

Commercial carbon nanotubes (mean diameter 10~20 nm, length 0.5~2 μm) were purchased from Chengdu Organic Chemicals Co., Ltd (Chengdu, China) and further modified via oxidation and sonication to obtain acid functionalized CNTs. Copper sulfate ($CuSO_4$•$5H_2O$) was obtained from Rgent Chemical Reagent Co., Ltd (Tianjin, China) as a copper source. Selenious dioxide (SeO_2) was supplied by Aladdin Chemistry Co., Ltd (Shanghai, China). Ascorbic acid (AA) was purchased from Dingguo Changsheng Biotechnology Co., Ltd (Beijing, China). Cetyltrimethyl ammonium bromide (CTAB) was supplied from Sinopharm Chemical Reagent Co., Ltd (Shanghai, China). Carboxyfluorescein diacetate succinimidyl ester (CFSE) were purchased from Dojindo Laboratories. 2′,7′-dichlorofluorescein diacetate (DCFH-DA) were purchased from Sigma. All chemical reagents were analytical grade. Milli-Q purified water (18.2 $M\Omega \cdot cm^{-1}$) was used throughout.

Apparatus

Ultraviolet and visible-near infrared absorption spectra were measured with a UV-3600 spectrophotometer (Hitachi Ltd., Tokyo, Japan). Transmission electron microscopy (TEM), high resolution transmission electron microscopy (HRTEM), and selected area electron diffraction (SAED) images were captured using a Tecnai G2 F20 S-TWIN microscopy (FEI, USA). Energy dispersive X-ray spectroscopy (EDX) and Scanning electron microscopy (SEM) images were obtianed with an S-4800 scanning electron microscope (Hitachi, Japan). X-ray photoelectron spectroscopy (XPS) analysis was performed with an ESCALAB 250 X-ray photoelectron spectrometer (Thermo, USA). Powder X-Ray diffraction (XRD) patterns were conducted on an XRD-7000 and filtered Cu Kα radiation in the range of 10~90° (2θ range). Zeta potential was measured using a Zatasizer Nano-ZS90 instrument (Malvern Inc). The photo-thermal property was monitored by a 980 nm NIR laser (power, 0.83W; laser spot diameter, 3 mm) and digital thermometer (accuracy 0.1°C), which were obtained from Hi-Tech Opto-electronics Co., Ltd. The optical density of HEp-2 cells cultured with samples at 450 nm was recorded by a Biotek Microplate Reader (USA). Flow cytometric analysis used BD FACSCalibur CellSorting System. The HEp-2 cells were imaged by an Olympus IX81LCS-DSU Disk Scanning con-focal microscope (Olympus, Japan).

Carboxylation of CNTs

Commercial carbon nanotubes were purified and functionalized according to the literature protocols.[25, 26] Briefly, 50 mg of CNTs was reuxed at 120 °C for 2 days under 100 mL of 2 M HNO_3 solution. After overnight proceed, the clear solution above the suspension was removed. Precipitation of CNTs were separated by centrifugation (12000 rpm, 30 min), and further oxidized by sonicating in a mixture of HNO_3 and H_2SO_4 (1:3, v/v) for 3 h. After the removal of the clear solution over the suspension, the precipitates were diluted by water and then filtered through 0.22 μm filtration membrane. Finally, the samples were further dried at 60°C under vacuum overnight to obtain accurate quantitative result and suspended as aqueous solutions of 1 mg•mL^{-1} for further use.

Preparation of $Cu_{2-x}Se$/CNTs

The $Cu_{2-x}Se$/CNTs nanohybrids were prepared according to our previous procedures with some improvements.[27, 28] In brief, carboxylic carbon nanotubes (100 μL, 1 mg•mL^{-1}) and 8 mL water were added to a round-bottom flask and then magnetically stirred with 1 mL CTAB (1 mg•mL^{-1}). Successively, 100 μL SeO_2 (0.1 M) and 200 μL AA (70 mg•mL^{-1}) was added into the above solution under vigorous stirring for 10 min. Afterwards a mixed solution of 200 μL $CuSO_4$ (0.1

M) and 800 μL AA (70 mg•mL^{-1}) was added to supply the catalytic reaction with Cu^{+}. The mixture was then kept vigorously stirring at 30°C for 1 h. After that, the temperature to 45°C was raised and further stirring was made for another 3 h until a deep atrovirens solution was obtained. The atrovirens solution of $Cu_{2-x}Se$/CNTs nano-hybrids was then transferred for centrifuge for 5 min at 10000 rpm and washing with distilled water alternately. Finally, the products were resuspended in water and stored in 4°C for further use. As a control, pure $Cu_{2-x}Se$ NPs were also prepared according to above procedures without CNTs.

In vitro cytotoxicity of $Cu_{2-x}Se$/CNTs

HEp-2 cells were added in the 96-well microtiter plate (1×10^5 cells per well) and cultured in RPMI 1640 medium supplemented with 2% fetal bovine serum at 37°C in a humidified incubator of 5% CO_2 for 24 h before the experiments. Then the cells were incubated with complete medium containing the $Cu_{2-x}Se$/CNTs nanohybrids at a series of concentrations (20, 30, 40, 50, 60, 70 μg•mL^{-1}) at 37 °C with 5% CO_2 for further 24 h and then they were rinsed with sterilized PBS twice. Subsequently, 90 μL FBS-free culture medium and 10 μL of CCK-8 solution were added to each well. After incubated for another 30 min, the optical density (OD) of each well was measured at 450 nm. Three replicates were done for each treatment group.

Measurement of photo-thermal performance

An aqueous suspension of $Cu_{2-x}Se$/CNTs (100 μL, 20, 40, 60, 80, 100 μg•mL^{-1}, respectively) was placed in 96-well microtiter plate and then irradiated by laser (wavelength, 980 nm; power, 0.83 W; laser spot diameter, 3 mm) for 15 min. The solution temperature was recorded through an IS-02B-USB digital thermometer every minute.

In vitro photo-thermal assay

Cells were plated in a 96-well plates with a density of 1.0×10^5 cells per well. After incubation for 24 h, the cells were washed with PBS and the $Cu_{2-x}Se$/CNTs nanohybrids (60 μg•mL^{-1}) suspended in medium were then added and cultured for 24 h. Finally, the HEp-2 cell were washed with PBS three times and irradiated by laser (wavelength, 980 nm; power, 0.83 W; laser spot diameter = 3 mm) for 15 min. After 24 h incubation, the cell viability was evaluated by CCK-8 assay. Similarly, the photo-thermal effect of $Cu_{2-x}Se$ NPs and CNTs were further curried out via MTT assay.

TUNEL-DAPI assay and flow cytometric analysis

HEp-2 Cells were seeded in glass bottom cell culture dishes (1×10^5 cells per dishes) for 24 h. Then cells were incubated with or without $Cu_{2-x}Se$/CNTs and NIR irradiation. Subsequently, the cells were fixed with 3.7% formaldehyde and 0.1% Triton X-100 in PBS solution, and then cultured with a TUNEL reaction mixture for 1 h and DAPI for 15 min at 37°C for DNA fragmentation and nuclear staining. Finally, the cells were imaged by the confocal microscope. For flow cytometric analysis, the HEp-2 cells were plated in a 6-well plate with a density of 2.0×10^5 cells per well. After treat with $Cu_{2-x}Se$/CNTs and 980 nm laser, the cells were collected and fixed with 70% ethanol at -20°C overnight. Finally, the cells were stained with propidium iodide (PI) and then the cell cycle distribution were futher investigated by flow cytometric analysis.

Photo-thermal ablation of HEp-2 cells

HEp-2 cells were cultured into glass bottom cell culture dishes (2×10^5 cells per dishes) for 24 h. The $Cu_{2-x}Se$/CNTs nanohybrids (60 μg•mL^{-1}) were then introduced separately to each dishes with complete medium. After 24 h incubation, the cells were washed with sterilized PBS twice to remove the free $Cu_{2-x}Se$/CNTs. Subsequently, the dishes were irradiated by laser (980 nm) for 15 min. After incubation for 24 h, the cell viability was assessed with 20 μM of carboxy-fluorescein succinimidyl ester (CFSE). The photo-thermal effect of $Cu_{2-x}Se$ NPs and CNTs were also evaluated by CFSE staining.

Imaging of intracellular reactive oxygen species (ROS)

The cells were seeded into glass bottom cell culture dishes (1×10^5 cells per dishes) for 24 h. Then the cells treated with $Cu_{2-x}Se$/CNTs or NIR irradiation. After incubition for 6 h and 12 h, the cells cultured with DCFH-DA probe for 30 min at 37°C (10 μM). The intracellular ROS level could reflect from the intensity of fluorescence by the confocal microscope.

Results and discussion

Characterization and LSPR properties of $Cu_{2-x}Se$/CNTs

The schematic illustration of the preparation process of $Cu_{2-x}Se$/CNTs nanohybrids is clearly displayed in Scheme 1. The commercial CNTs are sonicated and purified to obtaining short and low toxic nanotube. Because the long CNTs are hardly to enter the most cells and the motley metal catalyst residues used to prepare the commercial CNTs have been proven toxic.[29, 30] In order to possess good water dispersibility, CNTs are further modified with carboxyl and hydroxyl groups through strong acid treatment.[31] Furthermore, the acid-functionalized CNTs as a flexible one-dimensional carrier which can provide more functional groups for anchoring $Cu_{2-x}Se$ NPs. The TEM (Fig. 1A) images clearly show that the spherical $Cu_{2-x}Se$ NPs are uniformly with the particle sizes about 15~20 nm (Fig. 1B), and they are closely attached on the surface of the CNTs (Fig.

1C). There are not free nanoparticles in the field of vision, which shows a high laden efficiency of the acid-

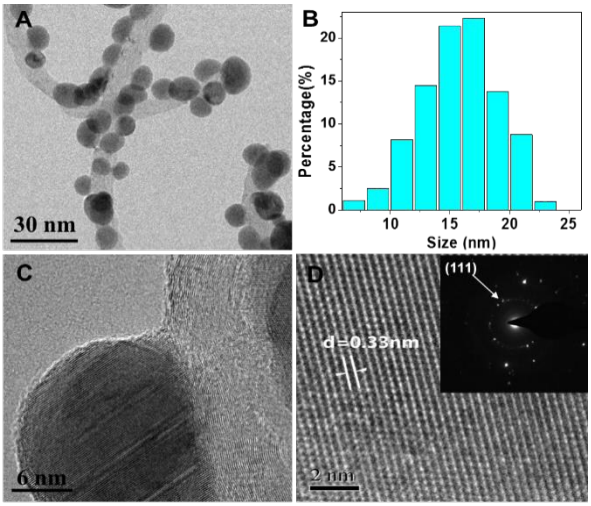

Fig. 1 The structures and morphologies of $Cu_{2-x}Se$/CNTs nanohybrids. (A) TEM image, (B) the particle sizes distribution histogram diagram of $Cu_{2-x}Se$ NPs on the surface of CNTs, (C) high magnified TEM images and (D) HRTEM image of $Cu_{2-x}Se$/CNTs nanohybrids and inset shows the SAED pattern of $Cu_{2-x}Se$/CNTs nanohybrids.

functionalized CNTs. The nanohybrids are also charac-terized by high-resolution TEM (HRTEM). The interplane distance of $Cu_{2-x}Se$ NPs is 0.33 nm (Fig. 1D), which is dominantly consistent with (111) crystalline planes[32] and the specific crystalline planes of $Cu_{2-x}Se$ NPs can be validated by the selected area electron diffraction (SAED) pattern.

The UV-vis-NIR absorption (Fig. 2A) measurements show that the $Cu_{2-x}Se$/CNTs nanohybrids exhibits a strong localized surface plasmon resonance absorption in the near-infrared region at 1055 nm, which should be assigned to the copper deficiencies in the $Cu_{2-x}Se$ NPs. [27, 28]. As a comparison, the pure $Cu_{2-x}Se$ NPs have the absorption band at 1035 nm, indicating that red-shifts of LSPR about 20 nm has occurred from the pure $Cu_{2-x}Se$ NPs to $Cu_{2-x}Se$/CNTs hybrids. The red-shifts may be attributed to the interaction of the polyaromatic surface of CNTs with the free carriers (holes) in the nonstoichiometric $Cu_{2-x}Se$ NPs and the $Cu_{2-x}Se$/CNTs are further excited to produce more electron-hole pairs under near-infrared irradiation.[33] Fig. 2B shows the FTIR spectra of CNTs and $Cu_{2-x}Se$/CNTs nanohybrids and the peaks at 3421, 1734 cm^{-1} are the oxygen-containing functional groups of carboxylated CNTs, which can be assigned to the –OH vibration and the C=O stretching vibration peaks. In addition, the bands at 1647 cm^{-1} is associated with the aromatic C=C skeletal vibrations of CNTs. Unexpectedly, the C=O stretching vibration peak disappear after the $Cu_{2-x}Se$ NPs in suit grow on the surface of CNTs. It is the difference between the spectrum of CNTs and $Cu_{2-x}Se$/CNTs nanohybrids, which evidence that the $Cu_{2-x}Se$ NPs may anchor on the acid-functionalized CNTs via carboxyl groups. In order to illustrate the formation process of $Cu_{2-x}Se$/CNTs, we further measure the ζ-potential in different reaction phases. In Fig. 2C, the potential of the acid functionalized CNTs is -41.3 mv and the aqueous solution of H_2SeO_3 perform a ζ-potential of 23.3 mV. The opposite charge make H_2SeO_3 propitiously combine with the CNTs through molecular electrostatic adhesion

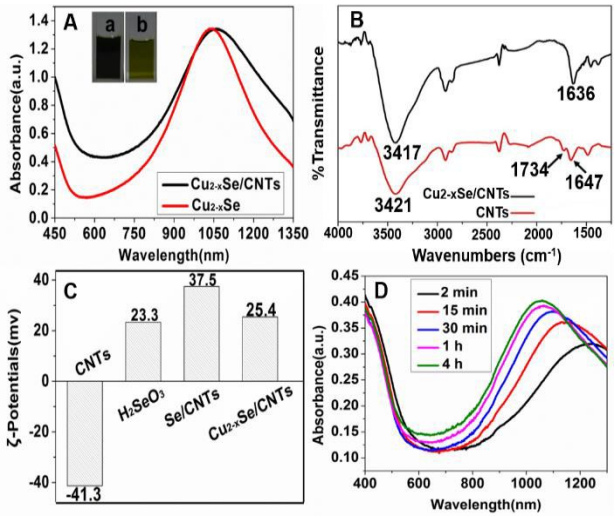

Fig. 2 The change of as-synthesized $Cu_{2-x}Se$/CNTs nanohybrids in absorption spectra and potential. (A) The UV-vis-NIR spectra of $Cu_{2-x}Se$ NPs and $Cu_{2-x}Se$/CNTs hybrids. The inserted pictures showed an aqueous dispersion of (a) $Cu_{2-x}Se$/CNTs nanohybrids and (b) $Cu_{2-x}Se$ NPs, (B) the FTIR spectra of CNTs and $Cu_{2-x}Se$/CNTs nanohybrids, (C) the ζ-potential analysis of $Cu_{2-x}Se$/CNTs nanohybrids, (D) optical absorption of $Cu_{2-x}Se$/CNTs nanohybrids synthesized for 2 min, 15 min, 30 min, 1 h and 4 h, respectively.

under vigorous stirring. After the addition of ascorbic acid, the H_2SeO_3 is reduced to Se NPs on the surface of CNTs (Se NPs/CNTs). However, the Se/CNTs in aqueous solutions are easily aggregated because of the high surface energy of Se NPs.[34] Therefore, we introduce some surfactant to reduce the surface energy and improve the stability. After the addition of CTAB, the ζ-potential of Se/CNTs is 37.5 mV and do not aggregate again. Finally, the $Cu_{2-x}Se$/CNTs possesses a ζ-potential of 25.4 mV when both $CuSO_4$ and AA are added. It is reported that Cu^{2+} immediately converted to Cu^{+} in the presence of AA and the role of Cu^{+} is to catalyze the Se^{0} to Se^{4+} and Se^{2-} and then combine with Se^{2-} to form Cu_2Se. [28, 35] Afterwards, the stoichiometric Cu_2Se was gradually oxidized and through a solid-state conversion to the nonstoichiometric $Cu_{2-x}Se$ with increasing oxygen exposure time under ambient conditions. [19, 36] As a result of the deeper level of copper deficiency, an intense LSPR band appears in the NIR characterized at 1055 nm. The LSPR band depends on the concentration of free carriers in the $Cu_{2-x}Se$/CNTs. The cationic Cu could escape from the crystal lattice, which forming cationic vacancies in the lattice and further creating free carriers (holes) in the NPs. [19, 37] With the extension of exposure to air, the free carrier density is increased and the NIR absorption spectra performed gradually enhancement and blue-shifts from 1235 nm to 1055 nm (Fig. 2D). [38]

The phase structures of the $Cu_{2-x}Se$/CNTs nanohybrids are also investigated via X-ray diffraction (XRD) patterns. In Fig. 3A, several well-defined diffraction peaks appears at 27.1°, 45.2° and 53.7°, which match with the (1, 1, 1), (2, 2, 0) and (3, 1, 1) planes of cubic $Cu_{2-x}Se$, referenced by standard $Cu_{2-x}Se$ phase (JCPDS card no: 06-0680). The result indicate that the phase structures of the $Cu_{2-x}Se$/CNTs nanohybrids are cubic crystal. Furthermore, $Cu_{2-x}Se$/CNTs nanohybrids emerge a wide and weak peak about 25°, which is clearly corresponding to the (002) plane of CNTs.[39] Fig. 3B presents the typical survey X-ray photoelectron spectroscopy spectrum of $Cu_{2-x}Se$/CNTs nanohybrids, which clearly shows the peaks of O 1s, C 1s and N 1s along with Cu 2p and Se 3d. The evolution of the Cu 2p XPS spectra at different reaction stage are performed. As illustrate in Fig. 3C, the XPS spectra shows a clear oxidation from Cu^+ to a mixture of Cu^+ and Cu^{2+}. The initial peaks of Cu $2p_{3/2}$ and Cu $2p_{1/2}$ are narrow, symmetric and without satellite peaks, which is indicative of monovalent copper in Cu_2Se sample. With a function of exposure time, the Cu 2p peaks are broadened and underwent splitting. In addition, the binding energies of Cu $2p_{3/2}$ and Cu $2p_{1/2}$ slightly shift to higher binding energy with an increase in exposure time near the typical values of 932.9 eV and 952.8 eV for Cu 2p in CuSe (Table. S1, ESI†).[40] The most notable of the Cu 2p XPS spectra is that a satellite line formed at 940~945 eV and its intensity are gradually pronounced with the process of reaction, resulting in the presence of paramagnetic Cu^{2+}.[18] The LSPR frequency depends on the free carriers (holes) in the nonstoichiometric NPs.[37] The results of Cu 2p XPS spectra reveal that the blue shift of the LSPR caused by a solid-state conversion to the nonstoichiometric $Cu_{2-x}Se$ with increasing oxygen exposure time under ambient conditions.[19, 38] The high resolution XPS spectrum of Se 3d is displayed in Fig. 3D. The peak at 54.6 eV is the binding energy of Se 3d (Se^{2-}) and along with a small peak at 58~60 eV owing to the high oxidation state of Se (Se^{4+}).[27]

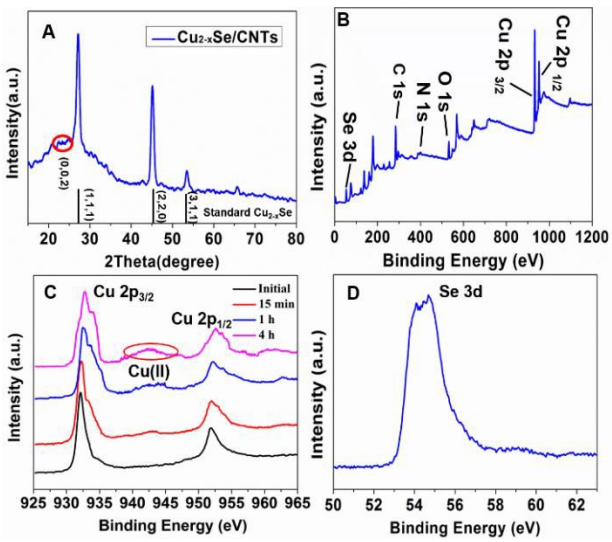

Fig. 3 The phase structures and valence state of the $Cu_{2-x}Se$/CNTs nanohybrids. (A) XRD patterns of the $Cu_{2-x}Se$/CNTs nanohybrids. Typical XPS spectra of the $Cu_{2-x}Se$/CNTs nanohybrids: (B) survey spectrum, (C) the evolution of the Cu 2p XPS spectra, (D) Se 3d region XPS spectrum.

For better elaborating the *in situ* preparation of $Cu_{2-x}Se$/CNTs nanohybrids, the morphology of $Cu_{2-x}Se$ NPs is also monitored at different reaction time. In Fig. 4 (A~D), the shape and size of $Cu_{2-x}Se$ NPs remain unchanged during the air exposure. The result is in good agreement with the literatures[27, 36] that the cation vacancies are produced in the crystal lattice and led to the formation of free carriers (holes), while the actual structure of the nanocrystal remains practically unperturbed with the extension of exposure to air. The Energy dispersive X-ray spectroscopy (EDX) analysis (Fig. 4E) further confirm the chemical composition of the $Cu_{2-x}Se$/CNTs nanohybrids, which show the existence of C, Cu and Se elements. Moreover, the atomic ratio of Cu/Se is close to 1.62 and associate with the high copper vacancy in $Cu_{2-x}Se$. [28]

The photo-thermal performance of $Cu_{2-x}Se$/CNTs

To evaluate the absorbing capacity of $Cu_{2-x}Se$ NPs, $Cu_{2-x}Se$/CNTs and CNTs in the near-infrared region, the UV-vis-NIR absorption spectral evolution of the nanocrystals with different concentrations are measured in Fig. 5A , 5B and 5C. It is clearly seen that the value of absorbance raise with the increase in the

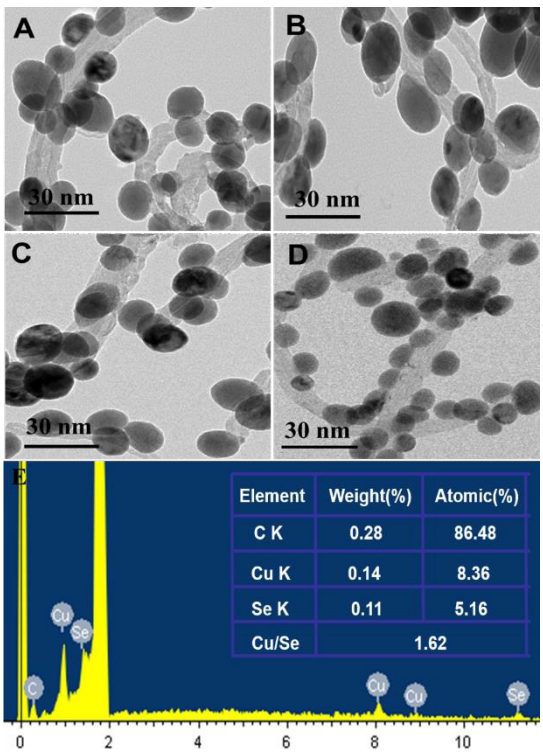

Fig. 4 The evolution of morphology and chemical composition of $Cu_{2-x}Se$/CNTs nanohybrids. TEM images of $Cu_{2-x}Se$/CNTs nanohybrids

synthesized for (A) 2 min, (B) 15 min, (C) 1 h, and (D) 4 h, respetively. (E) EDX spectra and the content of different elements of $Cu_{2-x}Se$/CNTs nanohybrids.

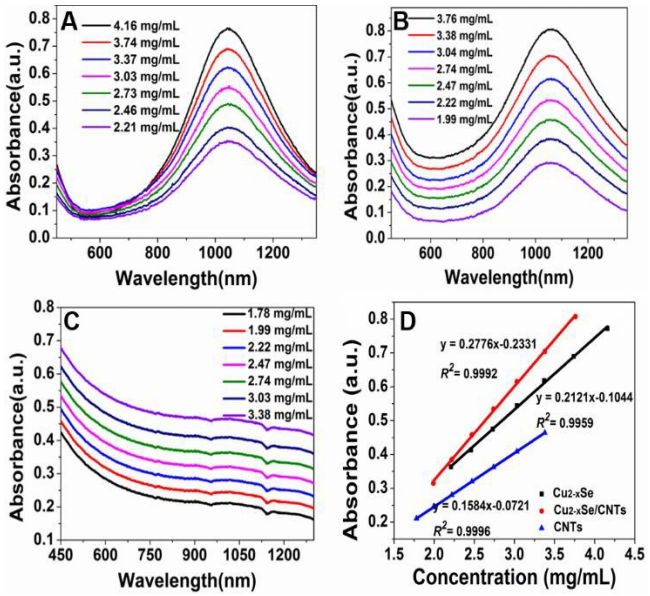

Fig. 5 The UV-vis-NIR absorption spectral evolution of the $Cu_{2-x}Se$ NPs (A), $Cu_{2-x}Se$/CNTs (B) and CNTs (C) with different concentrations. (D) the relationship between absorbance and the concentration of nanocrystals .

concentration of nanomaterials. The relationship between absorbance and the concentration of nanocrystals is showed in Fig. 5D, which export from the data of Fig. 5A , 5B and 5C, respectively. The results indicate that the absorbance maintain a good linear relationship with the concentration of nanomaterials and the slope of equation of $Cu_{2-x}Se$/CNTs (k = 0.2776) is significantly higher than $Cu_{2-x}Se$ NPs (k = 0.2121) and CNTs (k = 0.1584). In order to further compare their absorbency, the absorption co-efficient ($E^{1\%}_{1cm}$) at 980 nm is calculated from Fig. 5D on the basis of Lambert-Beer law ($A = E^{1\%}_{1cm}cl$) (Table. S2, ESI†). The result show that the absorption coefficient of $Cu_{2-x}Se$/CNTs nano-hybrids ($E^{1\%}_{1cm}$ = 1.921) is obviously greater than $Cu_{2-x}Se$ NPs ($E^{1\%}_{1cm}$ = 1.765) and CNTs ($E^{1\%}_{1cm}$ = 1.289). All the experimental data make clearly that the $Cu_{2-x}Se$/CNTs exhibit enhanced absorbing capacity than $Cu_{2-x}Se$ NPs and CNTs.

The strong intense LSPR band of $Cu_{2-x}Se$/CNTs nanohybrids appears in the near-infrared region indicates the possibility that the nanohybrids can be applied for photo-thermal therapy (PTT). To demonstrate the photo-thermal effect of as-prepared $Cu_{2-x}Se$/CNTs nanohybrids, we monitor the temperature of the aqueous solution containing various concentrations of $Cu_{2-x}Se$/CNTs nanohybrids. The photo-thermal effects of $Cu_{2-x}Se$/CNTs solution at different concentrations and time intervals are absolutely higher than those of pure water within 15 min, although the laser does not correspond the characteristic one of $Cu_{2-x}Se$/CNTs nanohybrids at 1055 nm (Fig. 6A). Furthermore, after irradiated by the NIR laser under the same conditions, the $Cu_{2-x}Se$/CNTs exhibit better photothermal effect than pure $Cu_{2-x}Se$ NPs and CNTs (Fig. 6B). From their UV-vis-NIR absorption (Fig. S1, ESI†), the CNTs reveal broad LSPR band over UV to NIR, but compared with $Cu_{2-x}Se$ and $Cu_{2-x}Se$/CNTs, it is no characteristic absorption peak in NIR, especially at 980 nm. Therefore, the heat generation depend on the combination of $Cu_{2-x}Se$ and CNTs, but it mainly contributed by the $Cu_{2-x}Se$ NPs. However, the introduction of CNTs still have some advantages in the improvement of photo-thermal performance. By combining the photo-thermal effects of CNT in the NIR region and the strong LSPR of $Cu_{2-x}Se$ NPs, the nanohybrids show an enhanced photo-thermal conversion ability than individual one. The plot of temperature change (ΔT) every three minutes versus different concentration of $Cu_{2-x}Se$/CNTs are exported from Fig. 6A. In all cases, the temperature change goes up significantly with an increase of $Cu_{2-x}Se$/CNTs nanohybrids concentration from 0 to 100 $\mu g \cdot mL^{-1}$ every minutes and tend to a platform when the irradiate time is extended to 15 min (Fig. 6C). This result should be attributed to the strong LSPR absorption of $Cu_{2-x}Se$/CNTs nanohybrids and fast heat loss at relatively high temperature. [23, 41] In addition, along with the extension of irradiate time, the absorption capacity of $Cu_{2-x}Se$/CNTs nanohybrids in the near infrared band is close to saturation, so the plot of temperature change tends to be flat. Because the ideal photo-thermal agent should be biocompatible for biological applications, the nanohybrids with different concentration were incubated with HEp-2 cell for 24 h. As shown in Fig. 6D, no obvious cytotoxicity in the concentration range of 20~70 $\mu g \cdot mL^{-1}$ as quantitatively evaluated by cell counting kit (CCK-8) assay and the data further prove the $Cu_{2-x}Se$/CNTs can become an ideal photo-thermal agent for ablation of cancer cells.

The photo-thermal assay of $Cu_{2-x}Se$/CNTs in vitro

In vitro photo-thermal performance of $Cu_{2-x}Se$/CNTs nano-

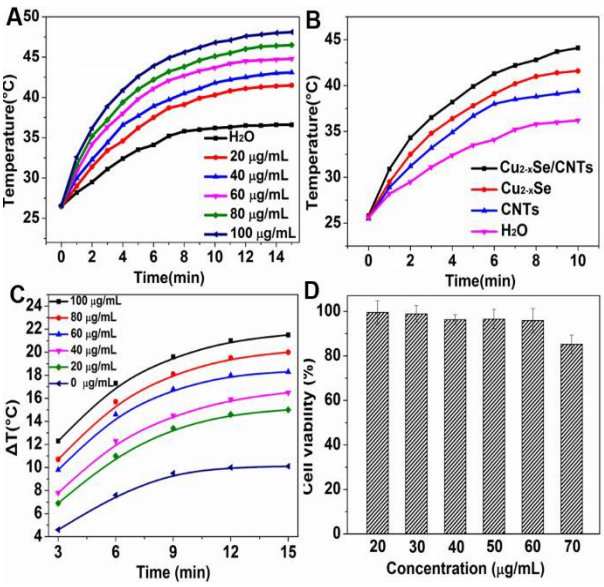

Fig. 6 The photo-thermal performance and cytotoxicity of the $Cu_{2-x}Se$/CNTs nanohybrids. (A) temperature change of pure water and aqueous dispersion of $Cu_{2-x}Se$/CNTs nanohybrids at different concentrations under irradiation of the 980 nm laser. (B) the photo-thermal curves of pure water, $Cu_{2-x}Se$ NPs, $Cu_{2-x}Se$/CNTs nanohybrids and CNTs with the same concentration under irradiation of the 980 nm laser. (C) plot of temperature change (ΔT) every three

minutes versus different concentration of $Cu_{2-x}Se$/CNTs. (D) the Cell viability after treatment with $Cu_{2-x}Se$/CNTs nanohybrids for 24 h.

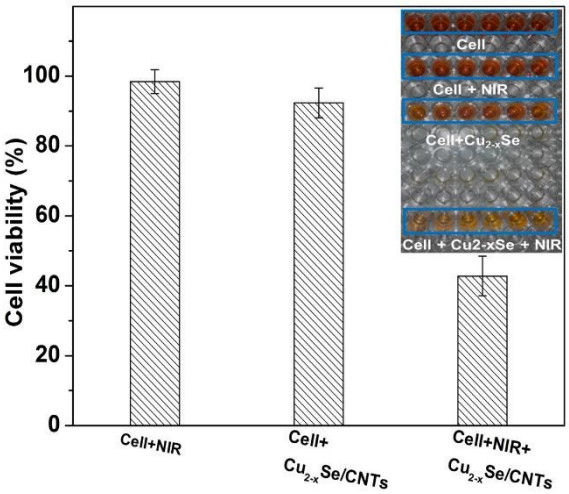

Fig. 7 The cell viability of HEp-2 cells incubated with or without $Cu_{2-x}Se$/CNTs nanohybrids under irradiation of the 980 nm laser and the inset shows the HEp-2 cells image explored with CCK-8 staining assay.

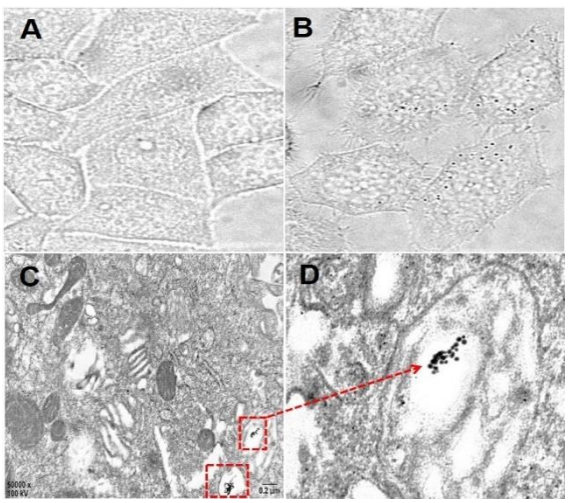

Fig. 8 The cellar uptake images of $Cu_{2-x}Se$/CNTs nanohybrids. (A) the control HEp-2 cell, (B) the cells incubated with $Cu_{2-x}Se$/CNTs for 24 h, (C) and (D) the high magnified region of cell uptake.

hybrids are explored with CCK-8 assay. As shown in Fig. 7, the cell viability can reduce to about 40% after treat with $Cu_{2-x}Se$/CNTs nanohybrids and 980 nm laser. The inset further evaluate the photo-thermal therapy effect of nanohybrids. It is obvious that the HEp-2 cells incubated with $Cu_{2-x}Se$/CNTs nanohybrids or processed with the 980 nm laser alone show obvious orange-yellow solution, which exhibit good biocompatibility of $Cu_{2-x}Se$/CNTs nanohybrids and further indicate that the cell cannot been damaged under this power (0.83 W). However, in presence of $Cu_{2-x}Se$/CNTs nanohybrids and irradiation of the 980 nm laser, the color of solution change to faint yellow. The results of CCK-8 assay exhibit the well photo-thermal therapy effect of $Cu_{2-x}Se$/CNTs nanohybrids *in vitro*.

The amount of nanomaterials uptaken by cancer cells is a crucial factor in photo-thermal therapy[8]. In such case, the HEp-2 cells are cultured into glass bottom cell culture dishes and incubated with $Cu_{2-x}Se$/CNTs nanohybrids for 24 h. Fig. 8A is the image of control HEp-2 cell and Fig. 8B is the cells incubated with $Cu_{2-x}Se$/CNTs for 24 h which can be clearly observed some black spots in the cell membrane. As a comparison, the control cells show relatively clean membrane. The black patches may be the $Cu_{2-x}Se$/CNTs nanohybrids or some agglomeration of the contrast agents. In order to confirm the black spots, the magnification TEM image of sectioned cells are obtained. As shown in Fig. 8C and 8D, it is obvious seen that the black patches are consisted of some nanoparticles, which further evidence the patches might be the $Cu_{2-x}Se$/CNTs nanohybrids. Finally, the result of elemental analysis clearly show the copper, selenium and carbon element (Fig. S2, ESI†), which confirm the existence of $Cu_{2-x}Se$/CNTs. The stability of $Cu_{2-x}Se$/CNTs structure is also important for photo-thermal therapy. Therefore, we treat the nanohybrids with ultra-sound for 1 h to investigate their stability. After ultrasonic treatment, the $Cu_{2-x}Se$ NPs remain anchored on the CNTs (Fig. S3, ESI†), which suggested the intense binding of $Cu_{2-x}Se$ NPs and CNTs. In addition, from the high magnification TEM image of sectioned cells, we can also find the complete structure of $Cu_{2-x}Se$/CNTs. Above images indicate the $Cu_{2-x}Se$/CNTs can be internalized by cells and the structure of $Cu_{2-x}Se$/CNTs is not broken after internalization into HEp-2 cells. The nanohybrids biodistribution in cells mainly locate at some cellular vesicles and subcellular organelles.

We further assess the photo-thermal therapy effects *in vitro* with carboxy-fluorescein succinimidyl ester (CFSE) staining assay. Living cells which can be stained in green fluorescence (Fig. 9A) and apoptotic cells are not affected

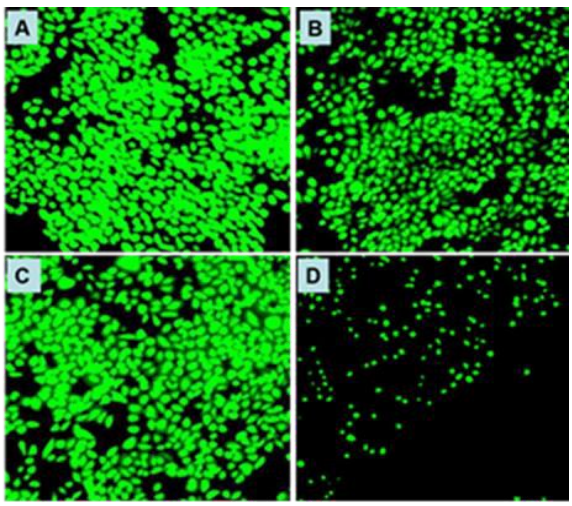

Fig. 9 Carboxy-fluorescein succinimidyl ester (CFSE) stained images of (A) HEp-2 cell, (B) HEp-2 cell incubated with $Cu_{2-x}Se$/CNTs nanohybrids (60 $\mu g \cdot mL^{-1}$) for 24 h, (C) HEp-2 cell treated with NIR laser (980 nm) for 15 min, (D) HEp-2 cells incubated with $Cu_{2-x}Se$/ CNTs

nanohybrids (60 μg•mL^{-1}) for 24 h and then irritated under a 980 nm laser for 15 min.

by the stain and keep neutral. The cells that incubate with $Cu_{2-x}Se$/CNTs nanohybrids (Fig. 9B) and treat with NIR laser (980 nm) alone (Fig. 9C) for 15 min remain keep green fluorescence. On the contrary, cultured with $Cu_{2-x}Se$/CNTs nanohybrids (60 μg•mL^{-1}) for 24 h and then subject to NIR irradiation for 15 min, the HEp-2 cells turn round and only a small amount of cells been stained by carboxy-fluorescein succinimidyl ester (Fig. 9D). On the basis of the results of Fig. 9A and 9B, it is further proved the good biocompatibility of $Cu_{2-x}Se$/CNTs. The Fig. 9C suggest that photo-thermal irritate under a 980 nm laser alone with safe power density. Finally, the morphology of HEp-2 cells show in Fig. 9D exhibit the excellent photo-thermal effect of $Cu_{2-x}Se$/ CNTs nanohybrids. All the data note that the $Cu_{2-x}Se$/CNTs nanohybrids with good biocompatibility can easily be internalized by cells, and then convert NIR laser into hyperpyrexia to change the cellular microenvironment.

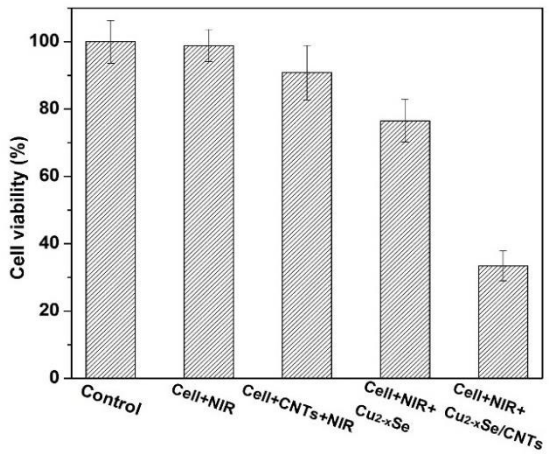

Fig. 10 The cell viability of HEp-2 cells incubated with CNTs, $Cu_{2-x}Se$ NPs and $Cu_{2-x}Se$/CNTs nanohybrids under irradiation of the 980 nm laser and explored with MTT staining assay.

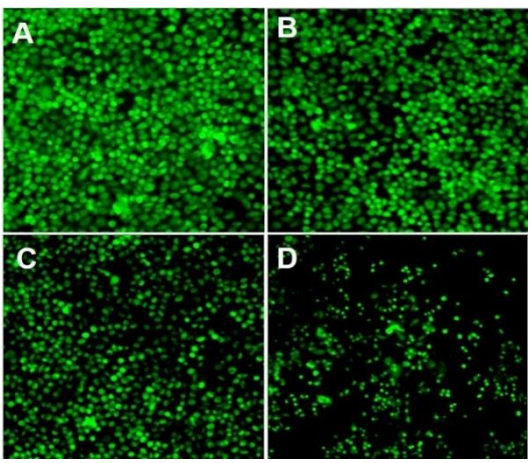

Fig. 11 CFSE stained images of (A) HEp-2 cell, (B) HEp-2 cell treated with CNTs (60 μg•mL^{-1}) for 24 h and NIR irritation for 15 min, (C) HEp-2 cell incubated with $Cu_{2-x}Se$ NPs (60 μg•mL^{-1}) and 980 nm laser, (D) HEp-2 cells cultured with $Cu_{2-x}Se$/CNTs nanohybrids (60 μg•mL^{-1}) for 24 h and then irritated for 15 min.

The nanohybrids can emerge as powerful agent for ablation of tumor cells.

Compared with individual CNTs and $Cu_{2-x}Se$ NPs, the $Cu_{2-x}Se$/CNTs nanohybrids also exhibit well photo-thermal therapy effect in cellular level. The cell viability under different conditions are also evaluated by MTT assay and CFSE staining assay. As illustration of Fig. 10, the HEp-2 cell treated with NIR laser (980 nm) alone or cultured with CNTs (60 μg•mL^{-1}) for 24 h and then subjected to NIR irradiation are no obvious cell toxicity, which reveal the safe laser power and the good biocompatibility of CNTs. The result also indicate that the CNTs cannot have ideal photo-thermal therapy effect at lower concentrations (60 μg•mL^{-1}). Furthermore, the cells viability of that treated with $Cu_{2-x}Se$ NPs (60 μg•mL^{-1}) and NIR irradiation exhibit small reduction, which attributed to the intense NIR absorption that generate heat to kill the cells, but the photo-thermal therapy effect is also not satisfactory. When the $Cu_{2-x}Se$/CNTs (60 μg•mL^{-1}) are incubated with cells and then subject to NIR irradiation, the cells viability show significant decrease (38.9%), which suggest that the $Cu_{2-x}Se$/CNTs possess outstanding photo-thermal therapy effect, compared with $Cu_{2-x}Se$ NPs and CNTs under the same conditions. In addition, we further culture cell with CFSE staining assay *in vitro*. Compared with the control group (Fig. 11A), the cells that treat with CNTs and NIR laser remain keep notable green fluorescence (Fig. 11B). However, the fluorescence of the cells culture with $Cu_{2-x}Se$ and NIR irradiation exhibit some decreases (Fig. 11C) and that of the group of the cell with $Cu_{2-x}Se$/CNTs and NIR laser are dramatically reduced (Fig. 11D) due to the form of apoptotic cells. Above CFSE staining images consistent with the result of MTT assay and the $Cu_{2-x}Se$/CNTs could become an ideal photo-thermal agent in cancer treatment.

Induction of apoptotic cell death by $Cu_{2-x}Se$/CNTs

In order to monitor the cellular death, we further do the following interpretation. At first, the cellular death is confirmed by TdT-mediated dUTP nick-end labeling (TU-

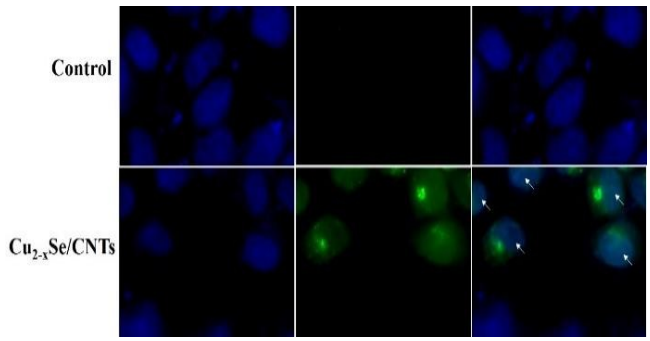

Fig. 12 The images of HEp-2 cells stained by TUNEL-DAPI after incubated with $Cu_{2-x}Se$/CNTs and NIR irradiation.

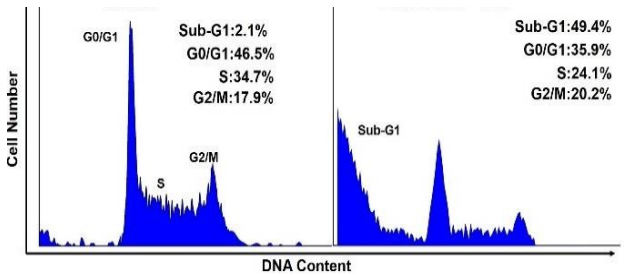

Fig. 13 The PI-flow cytometric analysis of HEp-2 cells exposed to $Cu_{2-x}Se$/CNTs and NIR irradiation.

NEL) and 4′,6-diamidino-2-phenylindole (DAPI) staining.

The DNA fragmentation of apoptotic cell can be labeled by TUNEL assay with green fluorescence and the nuclei of all cells can be stained by DAPI.[34] After the HEp-2 cells are incubated with $Cu_{2-x}Se$/CNTs and subject to NIR irradiation, the cellular nuclei is further treat with TUNEL-DAPI staining. In Fig. 12, compared with the control group, the treated cells can be labeled by TUNEL and the colocalization with DAPI exhibit well overlap (pointed by the arrows), which suggest the photo-thermal treated cells have already appeared apoptosis and lead to DNA fragmentation. In addition, we also investigate the cell cycle distribution to prove the cellular death by flow cytometric analysis. The result of propidium iodide (PI) flow cyto-metric analysis in Fig. 13 exhibit that the PI staining HEp-2 cells exposed to $Cu_{2-x}Se$/CNTs and NIR irradiation appeared a marked sub-G1 apoptotic peak, which further suggested the apoptotic cell death.[42]

Finally, according to the literature,[43-45] reactive oxygen species (ROS) is a kind of molecules containing oxygen,

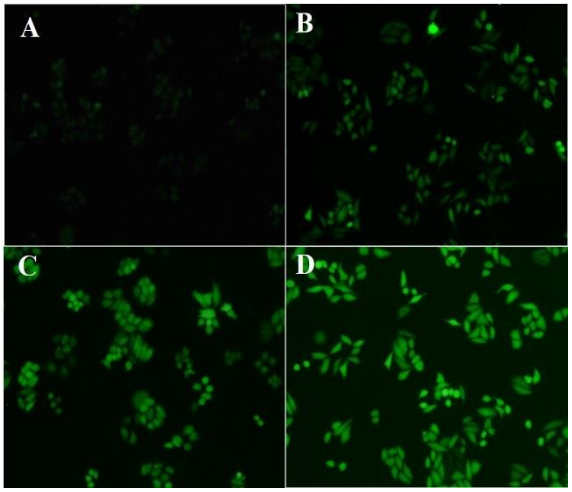

Fig. 14 The ROS images of HEp-2 cells stained by DCFH-DA probe. (A) control cells, (B) the cells cultured with $Cu_{2-x}Se$/CNTs, (C) the cells treated with $Cu_{2-x}Se$/CNTs and NIR irradiation and then further incubated for 6h. (D) the cells treated with $Cu_{2-x}Se$/ CNTs and NIR irradiation and then further incubated for 12h.

involve in hydroxyl radical, singlet oxygen, and peroxides and so on, which can lead to cell apoptosis and necrosis by cellular oxidative stress in the medium or high concentrations. Therefore, we further investigate the intracellular ROS generation in HEp-2 cells after the $Cu_{2-x}Se$/CNTs or NIR laser treatment and measured by 2′,7′-dichlorofluorescein diacetate (DCFH-DA). The non-fluorescent probe DCFH-DA can been hydrolysed by intracellular esterase and further oxidized to form DCF with green fluorescence. As shown in Fig. 14A, the cell in control group is no obvious green fluorescence after cultured with the DCFH-DA probe. However, the cells that incubated with $Cu_{2-x}Se$/CNTs and probe (Fig. 14B) exhibit weak fluorescence, suggesting the nanohybrids can create a small amount of ROS that may be caused by the stimulation of nanoparticles on cells. After treated with nanohybrids and NIR laser, the HEp-2 cells are further cultured for 6 h and 12 h and then the DCF fluorescence are imaged by confocal microscope. In Fig. 14C and 14D, it can be clearly observed that the fluorescence intensity is enhanced with the increase of the incubation time, which indicating the improvement of ROS level in cell after the laser irradiation. Above data reveal that the cell apoptosis may be attributed to the generation of heat and ROS and the $Cu_{2-x}Se$/CNTs nanohybrids will possess huge potential in feature cancer treatment.

CONCLUSIONS

In summary, the $Cu_{2-x}Se$/CNTs nanohybrids are successfully synthesized by a water-phase approach at room temperature, which show intense localized surface plasmon resonance in the near-infrared region. The functionalized carbon nanotubes as a carrier supply rich amino and carboxylic acid groups for the *in suit*

growth of $Cu_{2-x}Se$ nanoparticles, and the combination of carbon nanotubes enhance the absorbency and photo-thermal performance of $Cu_{2-x}Se$ NPs in the near-infrared region. Moreover, the hydrophilic nanohybrids possess excellent biocompatibility and tend to be internalized by cells. Importantly, the material can effectively kill cancer cells *in vitro* by the near-infrared radiation and reactive oxygen species generation, and therefore has a great potential use for cancer ablation.

Acknowledgements

This work was financially supported by the National Natural Science Foundation of China (NSFC, no. 21375109).

Notes and references

[a] Key Laboratory of Luminescent and Real-Time Analytical Chemistry (Southwest University), Ministry of Education, College of Pharma-ceutical Science, Southwest University, Chongqing 400715, China. *E-mail: chengzhi@swu.edu.cn*.

[b] College of Chemistry and Chemical Engineering, Southwest University, Chongqing 400715, China.

1 P. K. Jain, X. Huang, I. H. El-Sayed and M. A. El-Sayed, *Acc. Chem. Res.*, 2008, **41**, 1578-1586.
2 S. Lal, S. E. Clare and N. J. Halas, *Acc. Chem. Res.*, 2008, **41**, 1842-1851.
3 Q. Chen, C. Wang, Z. Zhan, W. He, Z. Cheng, Y. Li and Z. Liu, *Biomaterials*, 2014, **35**, 8206-8214.
4 H. Gong, L. Cheng, J. Xiang, H. Xu, L. Z. Feng, X. Z. Shi and Z. Liu, *Adv. Funct. Mater.*, 2013, **23**, 6059-6067.
5 U. Prabhakar, H. Maeda, R. K. Jain, E. M. Sevick-Muraca, W. Zamboni, O. C. Farokhzad, S. T. Barry, A. Gabizon, P. Grodzinski and D. C. Blakey, *Cancer Res.*, 2013, **73**, 2412-2417.
6 Z. Liu, S. Tabakman, K. Welsher and H. Dai, *Nano Res.*, 2009, **2**, 85-120.
7 K. Yang, S. Zhang, G. Zhang, X. Sun, S.-T. Lee and Z. Liu, *Nano Lett.*, 2010, **10**, 3318-3323.
8 S. Z. Nergiz, N. Gandra, S. Tadepalli and S. Singamaneni, *Acs Appl. Mater. Interfaces*, 2014, **6**, 16395-16402.
9. L. Meng, W. Xia, L. Liu, L. Niu and Q. Lu, *ACS Appl. Mater. Interfaces*, 2014, **6**, 4989-4996.
10 F. Schoppler, C. Mann, T. C. Hain, F. M. Neubauer, G. Privitera, F. Bonaccorso, D. P. Chu, A. C. Ferrari and T. Hertel, *J. Phys. Chem. C*, 2011, **115**, 14682-14686.
11 S. Link and M. A. El-Sayed, *Int. Rev. Phys. Chem.* , 2000, **19**, 409-453.
12 J. Yang, J. Choi, D. Bang, E. Kim, E. K. Lim, H. Park, J. S. Suh, K. Lee, K. H. Yoo, E. K. Kim, Y. M. Huh and S. Haam, *Angew. Chem. Int. Ed.*, 2011, **50**, 441-444.
13. W. R. Chen, R. L. Adams, A. K. Higgins, K. E. Bartels and R. E. Nordquist, *Cancer Lett.*, 1996, **98**, 169-173.
14. B. Nikoobakht, J. Wang and M. A. El-Sayed, *Chem. Phys. Lett.*, 2002, **366**, 17-23.
15 L. R. Hirsch, R. J. Stafford, J. A. Bankson, S. R. Sershen, B. Rivera, R. E. Price, J. D. Hazle, N. J. Halas and J. L. West, *Proc Natl Acad Sci U S A*, 2003, **100**, 13549-13554.
16 C. M. Hessel, V. P. Pattani, M. Rasch, M. G. Panthani, B. Koo, J. W. Tunnell and B. A. Korgel, *Nano Lett.*, 2011, **11**, 2560-2566.
17 Y. Zhao, H. Pan, Y. Lou, X. Qiu, J. Zhu and C. Burda, *J. Am. Chem. Soc.*, 2009, **131**, 4253-4261.
18 S. Deka, A. Genovese, Y. Zhang, K. Miszta, G. Bertoni, R. Krahne, C. Giannini and L. Manna, *J. Am. Chem. Soc.*, 2010, **132**, 8912-+.
19 I. Kriegel, C. Jiang, J. Rodríguez-Fernández, R. D. Schaller, D. V. Talapin, E. da Como and J. Feldmann, *J. Am. Chem. Soc.*, 2011, **134**, 1583-1590.
20 X. Liu, X. Wang, B. Zhou, W.-C. Law, A. N. Cartwright and M. T. Swihart, *Adv. Funct. Mater.*, 2013, **23**, 1256-1264.
21 C. Zhang, Y.-Y. Fu, X. Zhang, C. Yu, Y. Zhao and S.-K. Sun, *Dalton Trans*, 2015, **44**, 13112-13118.
22 G. Ku, M. Zhou, S. L. Song, Q. Huang, J. Hazle and C. Li, *Acs Nano*, 2012, **6**, 7489-7496.
23 Q. W. Tian, F. R. Jiang, R. J. Zou, Q. Liu, Z. G. Chen, M. F. Zhu, S. P. Yang, J. L. Wang, J. H. Wang and J. Q. Hu, *Acs Nano*, 2011, **5**, 9761-9771.
24 J. Han, H. Y. Zou, Z. X. Liu, T. Yang, M. X. Gao and C. Z. Huang, *New J. Chem.*, 2015, **39**, 6186-6192.
25 W. Wang, L. Zhan, Y. Q. Du, F. Leng, Y. Chang, M. X. Gao and C. Z. Huang, *Anal. Methods*, 2013, **5**, 5555-5559.
26 L. Zhang, S. J. Zhen, Y. Sang, J. Y. Li, Y. Wang, L. Zhan, L. Peng, J. Wang, Y. F. Li and C. Z. Huang, *Chem. Commun.*, 2010, **46**, 4303-4305.
27 W. L. Li, S. Q. Lie, Y. Q. Du, X. Y. Wan, T. T. Wang, J. Wang and C. Z. Huang, *J. Mater. Chem. B*, 2014, **2**, 7027-7033.
28 S. Q. Lie, D. M. Wang, M. X. Gao and C. Z. Huang, *Nanoscale*, 2014, **6**, 10289-10296.
29 X. Zhang, L. Meng, Q. Lu, Z. Fei and P. J. Dyson, *Biomaterials*, 2009, **30**, 6041-6047.
30 L. Meng, X. Zhang, Q. Lu, Z. Fei and P. J. Dyson, *Biomaterials*, 2012, **33**, 1689-1698.
31 P. G. He and M. Bayachou, *Langmuir*, 2005, **21**, 6086-6092.
32 J. Choi, N. Kang, H. Y. Yang, H. J. Kim and S. U. Son, *Chem. Mater.*, 2010, **22**, 3586-3588.
33 H. Wang, H.-L. Wang and W.-F. Jiang, *Chemosphere*, 2009, **75**, 1105-1111.
34 W. Liu, X. Li, Y.-S. Wong, W. Zheng, Y. Zhang, W. Cao and T. Chen, *ACS Nano*, 2012, **6**, 6578-6591.
35. F. X. Rong, Y. Bai, T. F. Chen and W. J. Zheng, *Mater. Res. Bull.*, 2012, **47**, 92-95.
36 D. Dorfs, T. Haertling, K. Miszta, N. C. Bigall, M. R. Kim, A. Genovese, A. Falqui, M. Povia and L. Manna, *J. Am. Chem. Soc.*, 2011, **133**, 11175-11180.
37 J. M. Luther, P. K. Jain, T. Ewers and A. P. Alivisatos, *Nat. Mater.*, 2011, **10**, 361-366.
38 S. C. Riha, D. C. Johnson and A. L. Prieto, *J. Am. Chem. Soc.*, 2010, **133**, 1383-1390.
39 W. Feng, M. Qin, P. Lv, J. Li and Y. Feng, *Carbon*, 2014, **77**, 1054-1064.
40 W. Shi, J. Shi, S. Yu and P. Liu, *Appl. Catal., B*, 2013, **138–139**, 184-190.
41 J. Hu, x. liu, Q. Wang, C. Li, R. Zou, B. Li, g. Song, K. Xu and Y. Zheng, *Nanoscale*, 2014, **6**, 4361-4370.
42 G. L. Hong, J. M. Liu, G. J. Zhao, J. P. Tan, B. Wu, M. F. Li, G. Liang, Q. M. Qiu and Z. Q. Lu, *J. Cell. Biochem.*, 2016, **117**, 872-880.
43 J. Wang and J. Yi, *Cancer Biol Ther*, 2008, **7**, 1875-1884.
44 F. Zhang, R. Xie, F. M. Munoz, S. S. Lau and T. J. Monks, *Toxicol. Sci.*, 2014, **140**, 118-134.
45 M. Brosché, T. Blomster, J. Salojärvi, F. Cui, N. Sipari, J. Leppälä, A. Lamminmäki, G. Tomai, S. Narayanasamy, R. A. Reddy, M. Keinänen, K. Overmyer and J. Kangasjärvi, *PLoS Genet*, 2014, **10**, e1004112.

A graphic abstract

for

Nonstoichiometric $Cu_{2-x}Se$ nanocrystals in situ produced on the surface of carbon nanotubes for ablation of tumor cells

Qiang Wang, [a] Wen Long Li, [b] Hong Yan Zou, [b] Hui Liu, *[a] and Cheng Zhi Huang *[ab]

a Key Laboratory of Luminescent and Real-Time Analytical Chemistry (Southwest University), Ministry of Education, College of Pharmaceutical Science, Southwest University, Chongqing 400715, China

b College of Chemistry and Chemical Engineering, Southwest University, Chongqing 400715, China

** Corresponding Author. E-mail: chengzhi@swu.edu.cn*

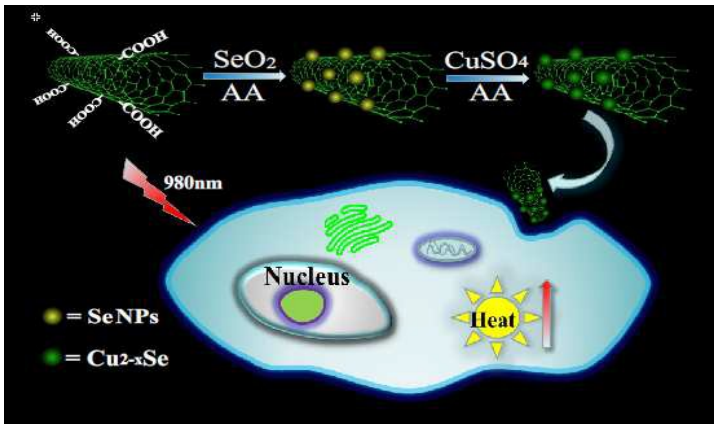

We fabricate $Cu_{2-x}Se$/CNTs nanohybrids with enhanced photo-thermal performance than individual one and further exploit them for ablation of cancer cells.